Composites: Part B 43 (2012) 1776–1784

Contents lists available at SciVerse ScienceDirect

Composites: Part B

journal homepage: www.elsevier.com/locate/compositesb

Analysis of mode I delamination of *z*-pinned composites using a non-dimensional analytical model

M.C. Song [a], B.V. Sankar [a,*], G. Subhash [a], C.F. Yen [b]

[a] Department of Mechanical and Aerospace Engineering, University of Florida, Gainesville, FL 32611, USA
[b] United States Army Research Laboratory, Aberdeen Proving Ground, MD 21005, USA

ARTICLE INFO

Article history:
Received 3 August 2011
Accepted 27 January 2012
Available online 9 February 2012

Keywords:
A. 3-Dimensional reinforcement
B. Delamination
C. Analytical modeling
C. Finite element analysis (FEA)
z-Pinning

ABSTRACT

We present a non-dimensional analytical model for crack propagation in a *z*-pinned double cantilever beam specimen (DCB) under mode I loading. Effect of various design parameters on the crack bridging length and apparent fracture toughness are investigated using this model. The efficacy of the analytical model is evaluated by comparing the results with 3D finite element (FE) simulations of the DCB. In the FE model the *z*-pins are modeled as discrete nonlinear elements. Bi-linear cohesive elements are used ahead of the crack tip to account for the interlaminar fracture toughness of the composite material. The results for load–deflection and crack length obtained from the analytical model and the FE model are compared and found to be in good agreement. The proposed non-dimensional analytical model will be useful in the design and analysis of translaminar reinforcements for composite structures.

1. Introduction

Composite materials are widely used in aerospace and automobile structures, sporting goods and military equipment since they show superior specific stiffness and strength. Delamination is one of the most significant damage modes in laminated composites and is a key element of consideration in design and operation. It is well known that translaminar reinforcements can enhance the delamination resistance and damage tolerance of composites significantly [1–4]. It is also known that sparse through-the-thickness reinforcements are not beneficial, and at the same time excessive amount of reinforcement is also deleterious as it results in damage to the composite structure and degradation in its properties [4]. The effect of *z*-fiber on delamination of composites has been extensively studied. Experimental approaches involve measurement of apparent fracture toughness [5], characterization of pull-out process of *z*-fiber [6,7] and crack propagation [7]. Analytic models are also available to find apparent fracture toughness and to establish the relationship among various design parameters [8–13]. Most analytic models used beam or plate models in which stitches are represented by an effective bridging force. Either Euler–Bernoulli beams [9–13] or Timoshenko beams [8,9] are used in association with discrete element [10] or continuous element [8,9,11–13] for the stitches. Numerical studies focused on crack initiation and progressive delamination in which J-integral [7], virtual crack closure technique (VCCT) [15] and cohesive zone method [14,16] were primarily used along with beam elements [14], plane strain elements [7], solid elements [16] or shell elements [15]. Sankar and Hu [17] used beam elements and spring elements similar to cohesive zone elements to simulate dynamic delamination propagation due to impact.

While FE models that account for each and every reinforcement may be more accurate in predicting the damage characteristics, they tend to be computationally expensive for realistic structures. On the other hand analytical models that smear the reinforcements as a continuous element are efficient and provide insight into the mechanics, but tend to be unrealistic in some situations.

A summary of past work in this area is provided in Table 1. In the following we briefly describe the salient features of the work listed in that table. Cartie [7] suggested a bi-linear bridging law through experiments and conducted FE simulation using plain strain elements. Robinson and Das [11], Mabson and Deobald [12] and Byrd and Birman [13] used linear softening bridging model whereas Ratcliffe and O'brien [10] proposed discrete element analytical model. For delamination modeling of *z*-pinned DCB, Dantuluri et al. [14] used 2D cohesive elements incorporating beam elements and a bi-linear bridging law. Ratcliffe and Krueger [16] used 3D cohesive model with solid elements. Grassi and Zhang [15] used VCCT for delamination modeling. It is clear from the table that various researchers have used different approaches in modeling the stated problem. Our goal here is to use both analytical and numerical approaches and compare them with available experimental data. In particular, we have developed a non-dimensional model that will be useful in the design of translaminar reinforcements for a given application. In particular we have used a 3D shell model

* Corresponding author.
E-mail address: sankar@ufl.edu (B.V. Sankar).

1359-8368/$ - see front matter © 2012 Elsevier Ltd. All rights reserved.
doi:10.1016/j.compositesb.2012.01.086

Table 1
Summary of results obtained by various researchers and present study.

Ref.	*z*-Pin in analytic model	*z*-Pin model in FEM	Crack propagation criterion in FEM	Sub-laminate model in FEM	Comparison with experimental data
Cartie [7]	–	Bi-linear traction	J integral	Plane strain	Yes
Mabson and Deobald [12]	Distributed force (non-dimensional form-1)	–	–	–	–
Byrd and Birman [13]	Distributed force (dimensional form-1)	–	–	–	–
Robinson and Das [11]	Distributed force (dimensional form-2)	–	–	–	Yes
Grassi and Zhang [15]	–	Nonlinear spring (bi-linear function)	VCCT	Shell element	Yes
Ratcliffe and O'brien [10]	Discrete force	–	–	–	Yes
Dantuluri et al. [14]	–	Nonlinear spring (bi-linear function)	2D cohesive element	Beam element	Yes
Ratcliffe and Krueger [16]	–	Nonlinear spring (bi-linear function)	3D cohesive element	Solid element	–
Present study	Distributed force (non-dimensional form-2)	Nonlinear spring (linear softening function and tri-linear bridging law)	3D cohesive element	Shell element	Yes

in conjunction with 3D cohesive elements. Both linear softening law and more realistic tri-linear bridging law are used to model the *z*-pins. In order to clarify the role of *z*-pins, a non-dimensional analytical model is proposed. The solution of the non-dimensional equation uses an iterative procedure. We have also derived an expression for the maximum density of *z*-pins that can be allowed before the beam fails otherwise. The efficacy of the analytical model is verified by finite element simulation of the DCB specimen. We have used the example given in [7] for this purpose. In the FE simulation, the ligaments of the DCB are modeled using shell elements. Cohesive elements are used to simulate the delamination and discrete nonlinear elements are used to model the *z*-pins. The agreement between the analytical model and FE simulations is found to be excellent for various results such as load–deflection, load-crack length, and effective fracture toughness.

It was found that steady-state bridging length and maximum apparent fracture toughness can be related to interlaminar fracture toughness of the composite and maximum frictional force supported by *z*-pins. The relationships among various parameters are non-dimensionalized and the maximum pin friction that can be allowed before the composite beam itself fails is calculated. The non-dimensional analytical model could be a useful design tool in selecting *z*-pins for composite structures to improve interlaminar fracture toughness.

2. Non-dimensional analytical model

Consider a *z*-pinned composite DCB specimen of thickness $2h$ with initial crack length of a_0 and subjected to Mode I loading as shown in Fig. 1a. A pair of transverse forces F is applied at the tip of the DCB. Due to the applied transverse force F the initial crack tends to reach the current crack length denoted by a (Fig. 1b). When the crack reaches the region reinforced by *z*-pins, a bridging zone of length c begins to develop (Fig. 1c). We can define an apparent crack length a_p which is the length of the crack up to the beginning of bridging zone. Current crack length (a) is the sum of the apparent crack length (a_p) and the bridging length (c). When the *z*-pins start to be completely pulled out of the composite as shown in Fig. 1d, the bridging zone becomes fully developed and a new fracture surface is created in the *z*-pinned zone. Therefore in the bridging zone

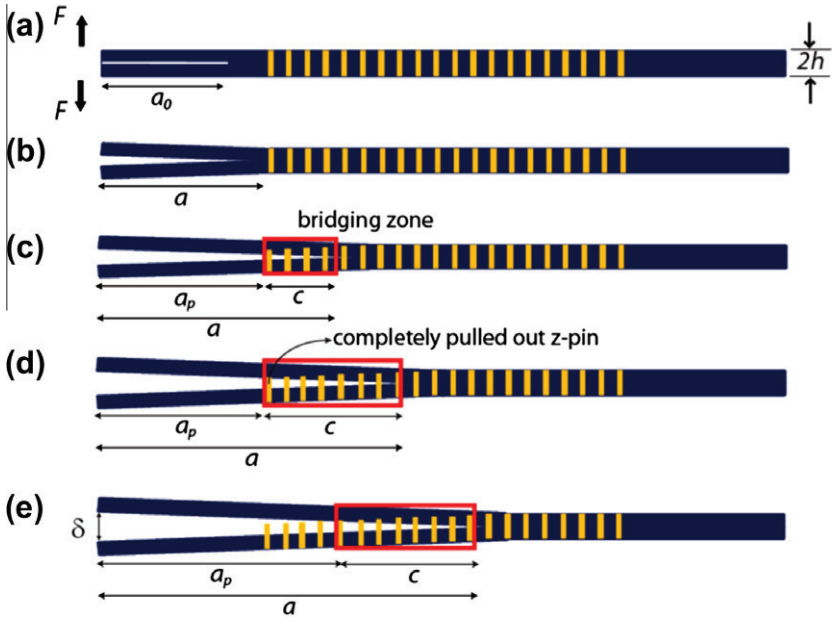

Fig. 1. Schematic of initial geometry and development of bridging zone by *z*-pins in the composite DCB.

the pull-out of pins is partial. Beyond the current crack tip the pins are assumed to be intact. The relative deflection at the tip of the DCB is denoted by δ as shown in Fig. 1e. Our goal is to determine the relationships among F, a, c, and δ. Once the bridging zone length c is determined other parameters such as F, a, and δ can be found by solving the governing equations. In the following we describe the non-dimensional equation governing the bridging zone and procedures to determine the bridging length for a given load.

We assume that the shear deformation is negligible and use Euler–Bernoulli beam equations to model the ligaments of the DCB as shown in Fig. 2b. We also assume that z-pins are rigid and there is sufficient friction between the z-pins and the composite material surrounding it. For simplicity, the relation between the frictional force (f) and pull out or slip distance (d_s) is idealized as a linear softening function as shown in Fig. 3. The validity of this assumption will be later verified in FE simulation. When the pins are intact they can exert a maximum friction force of f_m. As the pins pull out of the material, the loss of friction is proportional to the pullout distance d_s. When the pin is completely pulled out of the beam, the friction force reduces to zero. Thus the f–d_s relationship is given by:

$$f = f_m\left(1 - \frac{d_s}{h}\right), \quad 0 \leqslant d_s \leqslant h \tag{1}$$

where h is half the thickness of DCB.

Although the resistance offered by the pins on the beam is discreet, for the purpose of the analytical model we smear the discrete pin resistance as continuous distributed traction (p) acting on the crack surfaces as shown in Fig. 2c. Then the traction can be derived as:

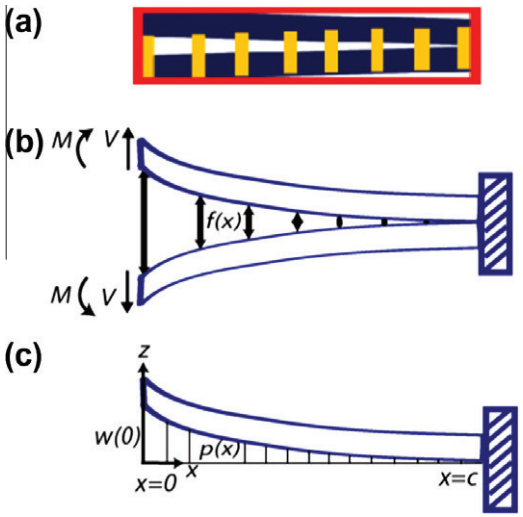

Fig. 2. Idealization of bridging zone using a beam model.

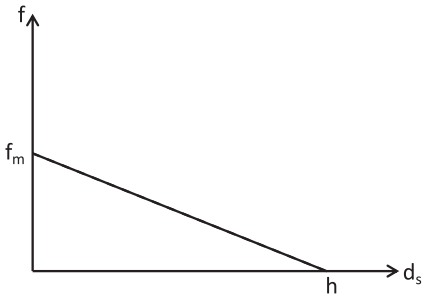

Fig. 3. Force–displacement relation of the z-pin.

$$p = Nf = Nf_m\left(1 - \frac{d_s}{h}\right) = p_m\left(1 - \frac{d_s}{h}\right) \tag{2}$$

where N is z-pin density expressed as number of z-pins per unit area.

The Euler–Bernoulli beam equation for one of the ligaments, say upper ligament (Fig. 2c), of the DCB can be written as:

$$EI\frac{d^4w}{dx^4} = -bp \tag{3}$$

where b is the beam width. The effective bending rigidity of one of the ligaments of the DCB is represented by the term EI. Note that the flexural rigidity for a laminated composite can be taken from the bending stiffness matrix in classical plate laminate theory. Substituting for p from Eq. (2) into Eq. (3), we obtain:

$$EI\frac{d^4w}{dx^4} - bp_m\frac{d_s}{h} = -bp_m \tag{4}$$

The pullout length d_s is equal to $2w$, where w is the deflection of the top or bottom beam. Hence, the governing equation takes the form:

$$EI\frac{d^4w}{dx^4} - 2p_m\frac{w}{h} = -bp_{\mathrm{m}} \tag{5}$$

The origin of the x-coordinate is assumed to be the point where the bridging zone begins. One should note that the origin moves as the crack propagates. The four boundary conditions (BCs) for bridging zone are:

$$\begin{aligned} &w(0) = w_0, \ (0 < w_0 \leqslant h/2) \\ &M_x(0) = a_p V_z(0) \ \Rightarrow \ \frac{d^2w}{dx^2}(0) = a_p\frac{d^3w}{dx^3}(0) \\ &w(c) = 0 \\ &\frac{dw}{dx}(c) = 0 \end{aligned} \tag{6}$$

In the above equation w_0 is a prescribed deflection at the origin of the coordinate system as shown in Fig. 2c. This value will be less than $h/2$ in the beginning and will increase to a maximum value of $h/2$ as the DCB is loaded. Note that the slip distance of the z-pin is equal to the total opening of the DCB at that location, i.e. $2w(x) = d_s(x)$. As the crack propagates, the bridging zone will also move with the crack, but the crack opening displacement will remain as h at the origin with $2w(0) = d_s(0) = h$. The terms V and M, respectively, are the bending moment and transverse shear force on the beam cross section.

One should note that the bridging length c is still an unknown. It can be determined from the fact that the strain energy release rate at the actual crack tip should be equal to the mode I fracture toughness at the instant of crack propagation. The energy release rate can be determined from the equation derived by Sankar and Sonik [18] for beam-like specimens containing delamination.

$$G = \frac{(M(c))^2}{bEI} = \frac{EI}{b}\left(\frac{d^2w(c)}{dx^2}\right)^2 \tag{7}$$

Thus the condition for determining c is:

$$\frac{EI}{b}\left(\frac{d^2w(c)}{dx^2}\right)^2 = G_{IC} \tag{8}$$

Before we solve the above equations we will non-dimensionalize the equations and BCs appropriately. Normalizing the length dimensions by h and forces by Eh^2, the governing equation and the BCs take the following form:

$$\frac{d^4\tilde{w}}{d\tilde{x}^4} - 2\tilde{p}_m\tilde{w} = -\tilde{p}_m \tag{9}$$

$$\begin{aligned} &\tilde{w}(0) = \tilde{w}_0, (0 < \tilde{w}_0 \leqslant 1/2) \\ &\frac{d^2\tilde{w}}{d\tilde{x}^2}(0) = \tilde{a}_p \frac{d^3\tilde{w}}{d\tilde{x}^3}(0) \\ &\tilde{w}(\tilde{c}) = 0 \\ &\frac{d\tilde{w}}{d\tilde{x}}(\tilde{c}) = 0 \end{aligned} \tag{10}$$

where

$$\tilde{x} = \frac{x}{h},\ \tilde{a}_p = \frac{a_p}{h},\ \tilde{c} = \frac{c}{h},\ \tilde{w} = \frac{w}{h} \text{ and } \tilde{p}_m = \frac{12p_m}{E}$$

The equation for determining $\tilde{c}$ (Eq. (8)) takes the form

$$\left(\frac{d^2\tilde{w}(\tilde{c})}{d\tilde{x}^2}\right)^2 = \tilde{G}_{IC} \tag{11}$$

where the non-dimensional fracture toughness is given by $\tilde{G}_{IC} = \frac{12G_{IC}}{Eh}$

The solution for the governing Eq. (9) is:

$$\tilde{w}(\tilde{x}) = C_1\cos\tilde{\lambda}\tilde{x} + C_2\sin\tilde{\lambda}\tilde{x} + C_3\cosh\tilde{\lambda}\tilde{x} + C_4\sinh\tilde{\lambda}\tilde{x} + \frac{1}{2} \tag{12}$$

where $\tilde{\lambda} = \sqrt[4]{2\tilde{p}_m}$

The boundary condition at the point $\tilde{x} = 0$ varies since deflection at this point $\tilde{w}_0$ increases from zero at the beginning of loading to 0.5 when the bridging zone is completely developed. Once the bridging zone is completely developed this value remains constant at 0.5 with additional increment of $\tilde{a}_p$. This is because the bridging zone is fully developed and it moves with the crack tip as it advances.

The procedures to solve the above set of equations are shown in the flow chart depicted in Fig. 4. The initial data includes the beam properties, characteristics of the *z*-pins and the fracture toughness G_{IC}. The deflection at the beginning of the bridging zone ($\tilde{x} = 0$) begins to increase as the load is applied.

When $\tilde{w}(0)$ = 0.5, bridging zone is fully developed and hereafter the deflection of the beginning of bridging zone is constant. However, the apparent crack length increases during crack propagation. We need to use an iterative procedure as the bridging length ($\tilde{c}$) is not known *a priori*. The strain energy release rate condition at the right end of the bridging zone ($\tilde{x} = \tilde{c}$) as given by Eq. (11) is then used to check for correct value of $\tilde{c}$. When a given $\tilde{c}$ satisfies Eq. (11), then the procedure to determine $\tilde{c}$ is terminated. After bridging zone is fully developed, bridging length corresponding to every increment of crack length can be determined.

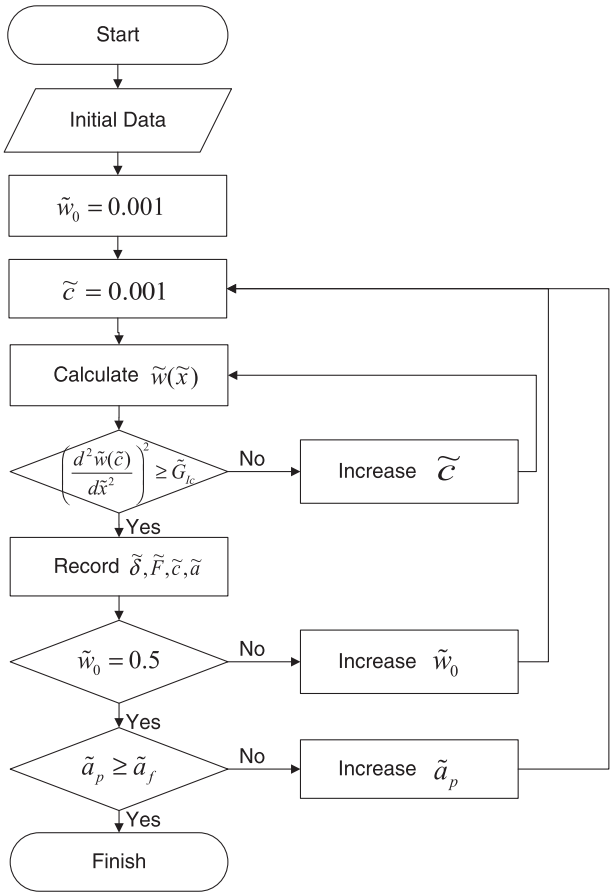

Fig. 4. Flowchart of the procedures for solving the non-dimensional governing equation.

3. Verification

3.1. Sample problem for verifying the non-dimensional analytical model

In order to verify the analytical model a *z*-pinned composites designed by Cartie [7] as shown in Fig. 5 was selected. This *z*-pinned composite was also used in many previous works [7,15]. The configurations and material properties are represented in Table 2. These values were used for both analytical model and FE simulation presented in the next section.

First, load–deflection curve (Fig. 6) was found for a_p values ranging from 52.25 mm to 62.25 mm. Meanwhile the crack length as the summation of the apparent crack length (a_p) and the bridging length (c) obtained from the procedure depicted in Fig. 4 was computed. The variation of the bridging length as a function of DCB deflection δ is shown in Fig. 7. The bridging length initially increases with loading until the bridging zone is fully developed, where the bridging length has the maximum value. In the beginning, the apparent crack length remains constant and the crack propagation is only due to evolution of the bridging zone. Once the bridging zone is fully developed there is little change in the bridging length thus the crack propagation is almost due to the apparent crack length. In fact there is a slight decrease in the bridging length after it reaches the maximum as the bending moment due to the transverse loads applied is a function of the apparent crack length. If a pair of couple is applied instead of a pair of forces as in the standard DCB test, then the bending moment will remain constant as the crack propagates, and one can see a steady state bridging length.

The force F acting on the DCB and opening displacement δ at the end of the beam can be obtained using the following relations:

$$F = -EI\left.\frac{d^3w}{dx^3}\right|_{x=0} \tag{13}$$

$$\delta = 2\left(w(0) + a_p\left.\frac{dw}{dx}\right|_{x=0} + \frac{1}{3}\left.\frac{d^3w}{dx^3}\right|_{x=0} a_p^3\right) \tag{14}$$

The variations of transverse force and crack length with increments in opening displacement are shown in Fig. 6. Initially the transverse force increases with opening displacement and begins to drop as interlaminar crack in unreinforced region propagates. However, the transverse force increases during the development of the bridging zone and decreases again with the movement of the fully developed bridging zone and the new crack surface.

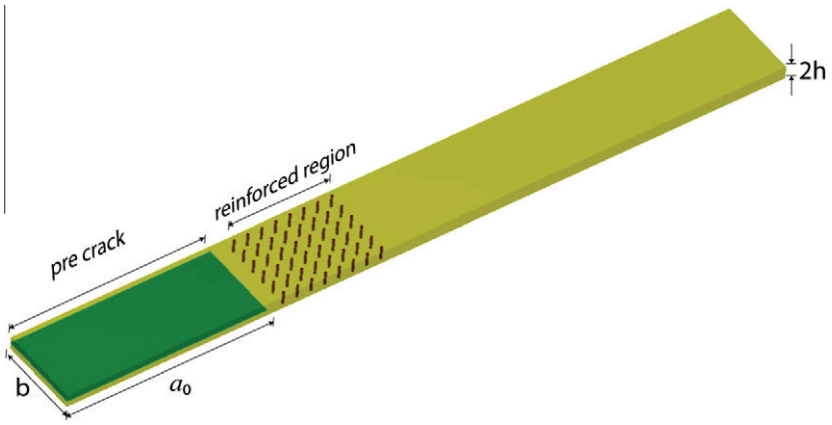

Fig. 5. DCB specimen reinforced by *z*-pins [7].

Table 2
The various dimensions and properties of the DCB used in the numerical simulation [6].

b	20 mm
h	1.6 mm
E_1	138 Gpa
E_2	11 GPa
ν_{12}	0.34
G_{12}	4.4 GPa
G_{Ic}	258 N/m
a_0	49 mm
F_m	18.43 N
z-Pin density	0.5%
z-Pin diameter	0.28 mm

In order to estimate the apparent fracture toughness during crack propagation we use bending moment at the apparent crack tip as a measure of increased fracture toughness. This is similar to calculating the fracture toughness of unreinforced beam using Eq. (7). Then the apparent fracture toughness is defined as:

$$G_{IC-app} = \frac{EI}{b}\left(\frac{d^2w(0)}{dx^2}\right)^2 \tag{15}$$

The above relation can be non-dimensionalized as:

$$\tilde{G}_{IC-app} = \left(\frac{d^2\tilde{w}(0)}{d\tilde{x}^2}\right)^2 \tag{16}$$

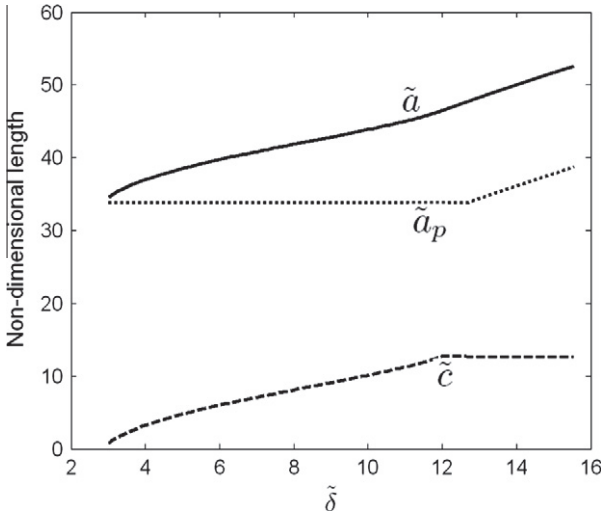

Fig. 7. Bridging length and crack length as a function of DCB deflection.

The variation of apparent fracture toughness during crack propagation is shown in Fig. 8. The apparent fracture toughness increases during development of the bridging length since the bending moment required at the beginning of bridging zone to

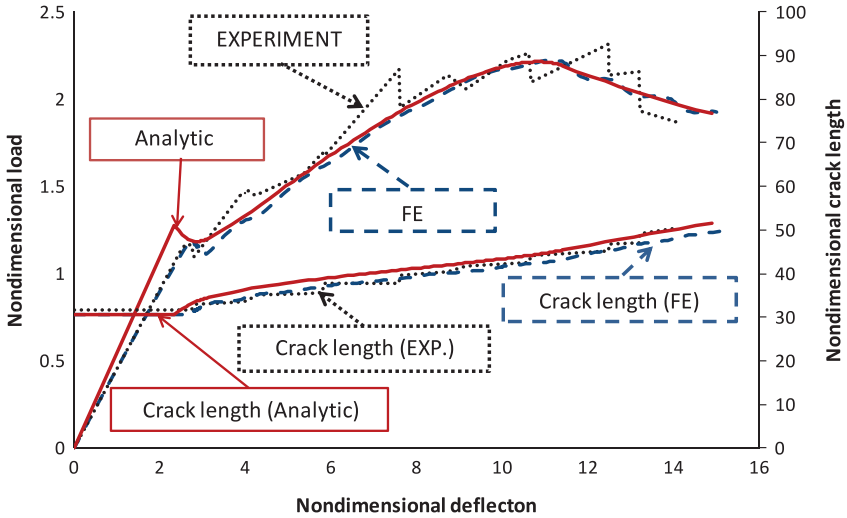

Fig. 6. Load and crack length variation as a function of DCB deflection.

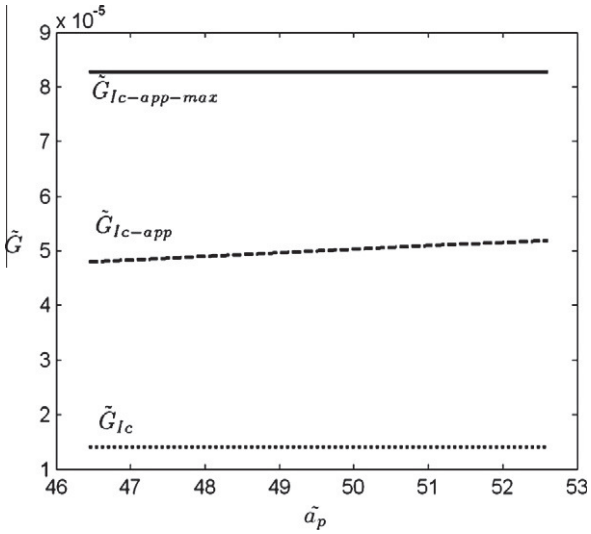

Fig. 8. Variation of apparent fracture toughness during crack propagation.

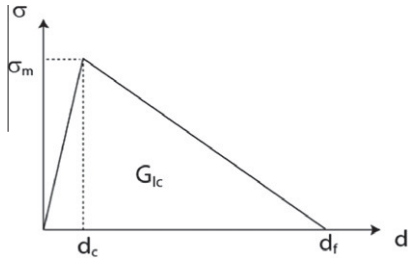

Fig. 9. Traction–separation law for the cohesive element.

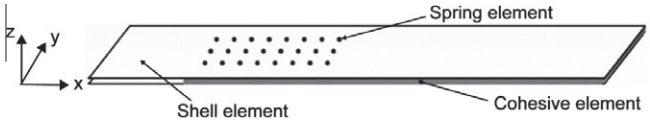

Fig. 10. Cohesive and spring elements in the FE model of the DCB.

overcome the bridging force is increases gradually. Maximum attainable apparent fracture toughness can be predicted by the relationship expressed in terms of interlaminar fracture toughness and bridging force due to *z*-pins. The relationship is exactly the same as the equation based on energy balance. As the crack propagates it has to overcome the frictional forces in the *z*-pins. The amount of extra work done is equal to the area under the load–deflection diagram in Fig. 3. Thus the maximum apparent fracture toughness can be derived as:

$$G_{IC-app-max} = G_{Ic} + N\left(\frac{1}{2} f_m h\right) \tag{17}$$

Multiplying throughout by $(12/Eh)$ we obtain the above relation in a non-dimensional form as:

$$\tilde{G}_{IC-app-max} = \tilde{G}_{Ic} + \frac{1}{2}\tilde{p}_m \tag{18}$$

This maximum value can be realized when a pair of couple is applied instead of a pair of transverse forces. As shown in Fig. 8 apparent fracture toughness for transverse loading is always less than the maximum value. Furthermore, our definition of apparent fracture toughness in Eq. (16) is also slightly different from the energy based relation given in Eq. (18) making the apparent fracture toughness under transverse loading less than the maximum realizable value. This is useful in evaluating the increase in apparent fracture toughness for a given design of *z*-pins. Moreover this value is related to strain exerted in the ligaments of DCB and will be discussed later.

3.2. FE simulation for verifying the non-dimensional analytical model

For the sake of comparison with the analytical model, FE simulation of the same specimen using the finite element software, ABAQUS®, was performed. The FE model containing discrete *z*-pins can verify the analytical model where *z*-pins are smeared and represented by distributed traction. The three-dimensional FE analysis was used to simulate crack propagation in the DCB specimen with *z*-pins. The specimen was modeled using shell elements (S4), and cohesive elements (COH3D8) were used to simulate progressive delamination.

The behavior of cohesive elements can be characterized by bilinear traction separation law (Fig. 9) [19] given by:

$$\sigma = (1-D)Kd$$

where

$$D = \begin{cases} 0, & d < d_0 \\ \frac{d_f(d-d_0)}{d(d_f-d_0)}, & d_0 < d < d_f \\ 1, & d_f < d \end{cases} \tag{19}$$

where σ is traction, K is stiffness, D is damage variable, d is displacement, d_0 is displacement at damage initiation and d_f is final displacement .

The above parameters were taken as: $K = 10^6$ N/mm, $\sigma_m = 35$ Mpa and $G_{IC} = 0.258$ N/mm [7,19].

Nonlinear spring element (CONN3D2) whose behavior is defined by linearly decreasing force (Fig. 3) for each *z*-pin was also implemented between the two ligaments of the DCB (Fig. 10).

The load–deflection curves and the variations of crack lengths with deflection are shown in Fig. 6. Both FE and analytical model results are presented with that from the experiment by Cartie [6]. The agreement between the analytical model and the FE simulations is satisfactory for both load–deflection and delamination length. The slight discrepancy in the initial slope of the load–deflection curve between the analytical model and the FE model is due to the fact that the analytical model uses Euler–Bernoulli beam theory whereas FE model considered shear deformation as it occurs in test specimens. The good comparison between the analytical model and the results from FEA and experiments suggests that the discrete bridging force can be represented by a distributed traction.

4. Discussion of results from the non-dimensional model

4.1. Parametric studies using the non-dimensional analytical model

Our goal was to study the effects of inherent interlaminar fracture toughness of the composite material $\tilde{G}_{Ic}$ and the non-dimensional frictional force $\tilde{p}_m$ on (i) the maximum apparent fracture toughness $\tilde{G}_{Ic-app-max}$ and (ii) steady state bridging length $\tilde{c}$. Such relationships are extremely useful in design process to evaluate the influence of design variables on performance of the composite. In this parametric study we assume that the DCB is loaded by end couples instead of transverse forces. This assures steady state crack propagation in the beam and effect of increasing crack length on the results is thus eliminated. In the simulations, $\tilde{G}_{Ic}$ is varied from 10^{-7} to10^{-4} and $\tilde{p}_m$ ranged from 10^{-10} (almost zero friction representing the case of unreinforced beam) to 0.1.

Fig. 11 shows that the steady state bridging length decreases with increasing $\tilde{G}_{Ic}$ and $\tilde{p}_m$. If the composite material is inherently

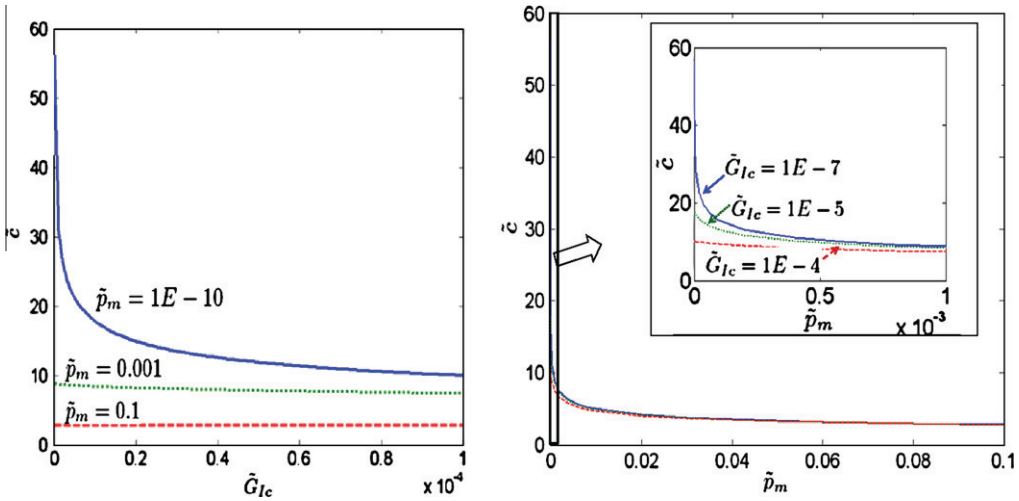

Fig. 11. Non-dimensional steady state bridging length.

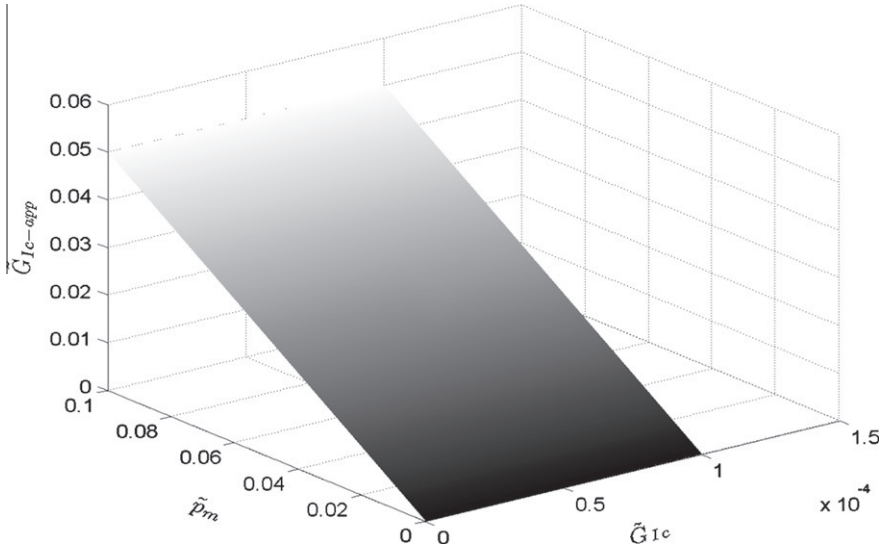

Fig. 12. Apparent fracture toughness as a function of maximum friction force and interlaminar fracture toughness.

tough, it will not allow a larger bridging length. Similarly a large friction force also will reduce the bridging length. The maximum apparent fracture toughness ($\widetilde{G}_{Ic-app-max}$) is another measure to evaluate the effect of translaminar reinforcement. Fig. 12 shows that the maximum apparent fracture toughness, computed by Eq. (16), varies linearly with increasing $\widetilde{G}_{ic-app-max}$ and $\tilde{p}_m$. This result is in accordance with Eq. (18). Since the range of $\tilde{p}_m$ is wider than that of $\widetilde{G}_{Ic}$ in reality, $\widetilde{G}_{Ic-app-max}$ is more sensitive to the value of $\tilde{p}_m$.

In other words the apparent fracture toughness is dominated by the translaminar reinforcement. From the results shown in Figs. 11 and 12, it is clear that higher friction force exerted by the z-pins provides enhanced fracture toughness and at the same time reduces the bridging length. The latter is important to maintain the stiffness of the structure for a larger bridging length leads to reduction in the stiffness of the structure.

4.2. Maximum allowable translaminar reinforcement

Even though large frictional force between the z-pin and the surrounding matrix material is desirable for increased fracture toughness, a frictional force beyond a critical value will cause the beam to fail. The maximum normal strain in a beam cross section is given by

$$\varepsilon_{\max} = \frac{h}{2}\left|\frac{d^2w}{dx^2}\right| \tag{20}$$

Note the strain is already non-dimensional and the right hand side of the above equation can be written as:

$$\varepsilon_{\max} = \frac{1}{2}\left|\frac{d^2\tilde{w}}{d\tilde{x}^2}\right| = \frac{\tilde{\kappa}}{2} \tag{21}$$

where $\tilde{\kappa}$ is the non-dimensional curvature which has the maximum value at $\tilde{x} = 0$. Using Eqs. (16) and (18) we obtain

$$\tilde{\kappa} = \sqrt{\widetilde{G}_{Ic} + \frac{1}{2}\tilde{p}_m} \tag{22}$$

Let us assume the allowable strain in the composite is given by ε_u.

Then,

$$\sqrt{\widetilde{G}_{Ic} + \frac{1}{2}\tilde{p}_m} < 2\varepsilon_u \tag{23}$$

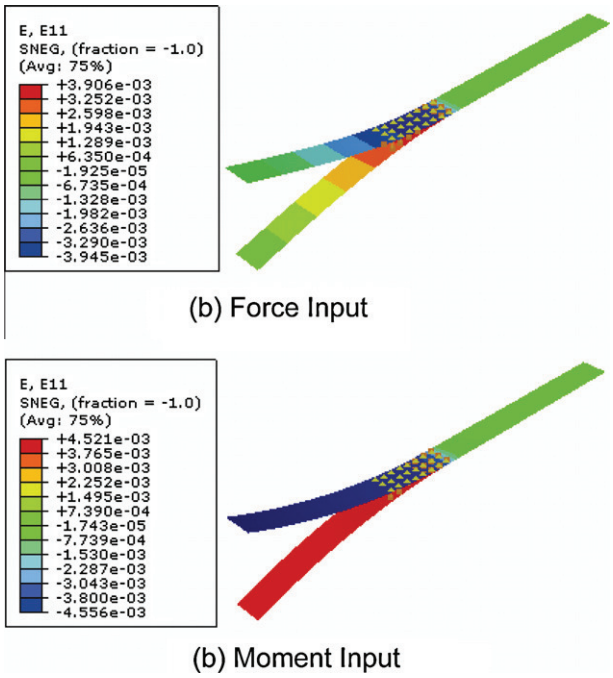

Fig. 13. Comparison of strain with different loading types.

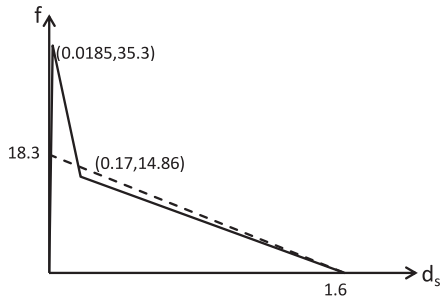

Fig. 14. Tri-linear bridging law is indicated by solid line. The dotted line is the linear softening law in Fig. 3. The areas under the force–displacement diagram for both laws are the same.

From the above equation one can derive

$$\tilde{p}_m < 2(4\varepsilon_u^2 - \tilde{G}_{Ic}) \quad \text{or} \quad p_m = Nf_m < \tfrac{2}{3}E\varepsilon_u^2 - \tfrac{2G_{Ic}}{h} \tag{24}$$

The above equation provides an upper limit on the z-pin density which should be taken into consideration in the design of translaminar reinforcements. Thus the allowable density or maximum frictional force of z-pins can be determined at a given geometry and material properties of a composite material.

In order to verify the result for the maximum allowable translaminar reinforcement given in Eq. (24), we performed finite element analysis of a specimen. The properties used were: $G_{Ic} = 0.258$ N/mm, $h = 1.6$ mm, $E = 138$ GPa, $Nf_m = 1.58$ N/mm^2 [7], The FE simulation was used to calculate the maximum strain in the ligaments of the DCB specimen at the instant of crack propagation, and it was compared with the ε_u obtained from Eq. (24). Two loading cases, namely end couples and transverse forces, were considered. For the set of properties used Eq. (24) yields a maximum strain $\varepsilon_u = 4.5 \times 10^{-3}$. Note that if $Nf_m > 1.58$ N/mm^2 then the maximum strain exceeds the ultimate strain. From the FE simulations we obtained $\varepsilon_{max} = 4.521 \times 10^{-3}$ for the case of end couples and $\varepsilon_{max} = 3.906 \times 10^{-3}$ for the case of transverse loading of the DCB (Fig. 13). The results indicate the strains in the beam are higher for the moment loading compared to that due to the transverse loading. However, in a practical structure the delamination will experience a combination of shear and moment loadings, and hence the conservative value should be used. That means the maximum allowable stitch density given in Eq. (24) should be used although it is applicable only to moment loading case, and hence conservative.

4.3. Effect of tri-linear bridging law

So far we have used the linear softening bridging law for developing the non-dimensional analytical model and verifying the same using FEA. Although this bridging law is simple, it may not be realistic. Dai et al. [6] performed pull-out tests using z-pins of various diameters to determine the actual bridging law. They found that a high value of debonding force was reached before the debonding of the pins began. After the debonding was initiated, the pull-out force dropped to a lower value before reducing linearly to zero value as the pins were pulled out steadily against frictional force that seemed to have a constant coefficient of friction. They represented this pullout behavior by a tri-linear bridging law as depicted in Fig. 14. The tri-linear behavior can be attributed to an elastic deformation (from (0, 0) to (0.0185, 35.3) in Fig. 14), debonding from surrounding matrix (from (0.0185, 35.3) to (0.17, 14.86) in Fig. 14) and slip-out of z-pins (from (0.17, 14.86) to (1.6, 0) in Fig. 14).

The finite element simulations of the DCB described in Section 3.2 were repeated with the tri-linear bridging law. We did not at-

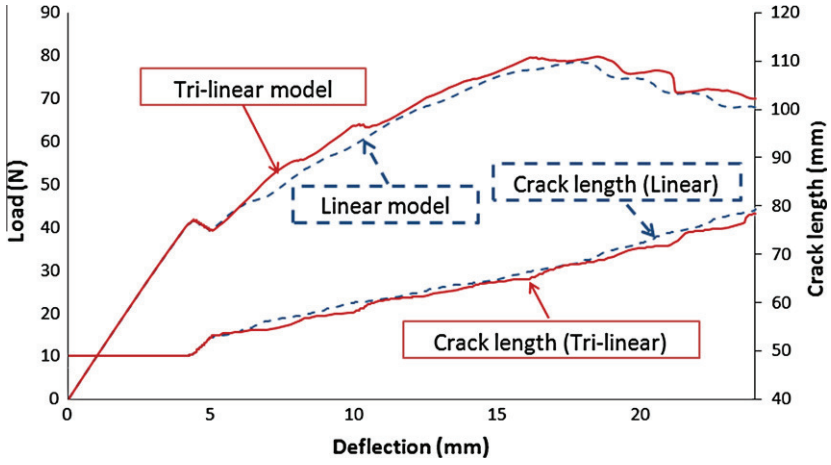

Fig. 15. Load–deflection curve from various bridging laws.

tempt analytical solution as it will be very complicated due to the piecewise continuous bridging law. The numerical values for the tri-linear law were chosen such that the area under the force–displacement curve, which is related to the increase in fracture toughness, is equal to the linear softening law used in the earlier example. That is the areas under the two force–displacement curves in Fig. 14 are equal to each other. The resulting load–deflection diagram of the *z*-pinned DCB specimen is shown in Fig. 15. The load deflection behavior is almost identical to that obtained using the linear bridging law indicating that the apparent fracture toughness is same in both cases. It must be noted that the peak force in the tri-linear case is almost twice as that of the linear softening law. The variations of crack length as a function of the DCB specimen opening (deflection) are also similar in both cases. This indicates that the details of the bridging law do not seem to affect the global behavior of the specimen as long as the energy dissipated by the pins is properly accounted for.

5. Summary and conclusions

Mode I delamination propagation in DCB specimens containing *z*-pins is studied. A simple analytical model based on linear softening type bridging law for the *z*-pins has been developed and suitable non-dimensional parameters have been identified. The load–deflection curve of the DCB specimen was calculated using the analytical model. It is seen that the bridging zone, wherein the pins are partially pulled out, develops as the crack propagates, but attains a steady state value. The length of the bridging zone is a function of the mode I fracture toughness and the frictional force between the *z*-pins and the surrounding material. An expression was derived for the apparent or effective fracture toughness values. Although increase in frictional force as the *z*-pins increases the fracture toughness, there is an upper limit to this friction as the DCB ligaments would break if the friction is very high. The limiting value of the pin friction is derived.

The efficacy of the analytical model was evaluated by the simulation of the DCB specimen using finite element simulations. In the FE model the delamination propagation was simulated by cohesive elements and the *z*-pins were modeled as discrete nonlinear elements. The results for load–deflection curve and the crack bridging zone length agreed quite well with the analytical model. As an alternative to the linear bridging law, a more realistic tri-linear bridging law was used in the FE simulations. It is found that the global delamination behavior of the specimen was not affected much as long as the energy dissipated by the pins is kept the same.

The non-dimensional model with few parameters will serve as a design tool when translaminar reinforcements such as *z*-pins are selected for laminated composite structures in order to improve their fracture toughness. The analytical models will also be useful in optimization studies and simulation of large composite structures containing translaminar reinforcements.

Acknowledgments

The funding for this work was provided by the United States Army Research Office(Grant No. W911NF-08-1-0120) and the United States Army Research Laboratory. The authors also would like to thank Dr. James G. Ratcliff at the National Institute for Aerospace, Hampton, VA for the discussion of results.

References

[1] Sharma SK, Sankar BV. Effects of through-the-thickness stitching on impact and interlaminar fracture properties of textile graphite/epoxy laminates. NASA CR-195042; 1995.
[2] Sankar BV, Sharma SK. Mode II delamination toughness of stitched graphite/epoxy textile composites. Compos Sci Technol 2002;62:1407–14.
[3] Jain LK, Mai YW. On the effect of stitching on mode I delamination toughness of laminated composites. Compos Sci Technol 1997;57:729–37.
[4] Mouritz AP. Review of *z*-pinned composite laminate. Compos Part A Appl Sci 2007;38:2383–97.
[5] Chen L, Sankar BV, Ifju PG. A new mode I fracture test for composites with translaminar reinforcements. Compos Sci Technol 2002;62:1407–14.
[6] Dai SC, Yan W, Liu HY, Mai YW. Experimental study on *z*-pin bridging law by pullout test. Compos Sci Technol 2004;64:2451–7.
[7] Cartie DDR. Effect of *z*-fibres™ on the delamination behaviour of carbon-fibre/epoxy laminates. PhD thesis. Cranfield University, UK; 2000.
[8] Sankar BV, Dharmapuri SM. Analysis of a stitched double cantilever beam. J Compos Mater 1998;32:2204–25.
[9] Sridhar N, Massabo R, Cox BN, Beyerlein IJ. Delamination dynamics in through-thickness reinforced laminates with application to DCB specimen delaminated composite beams. Int J Fract 2002;118:119–44.
[10] Ratcliffe JG, O'brien TK. Discrete spring model for predicting delamination growth in *z*-fiber reinforced DCB specimens. NASA/TM-2004-213019, ARL-TR-3190; 2004.
[11] Robinson P, Das S. Mode I DCB testing of composite laminates reinforced with *z*-direction pins: a simple model for the investigation of data reduction strategies. Eng Fract Mech 2004;71:345–64.
[12] Mabson GE, Deobald LR. Design curves for 3d reinforcement laminated double cantilever beams. In: Proceedings of mechanics of sandwich structure ASME 2000; 2000. p. 89–99.
[13] Byrd LW, Birman V. The estimate of the effect of *z*-pins on the strain release rate, fracture and fatigue in a composite co-cured *z*-pinned double cantilever beam. Compos Struct 2005;68:53–63.
[14] Dantuluri V, Maiti S, Geubelle PH, Patel R, Kilic H. Cohesive modeling of delamination in *z*-pin reinforced composite laminates. Compos Sci Technol 2007;67:616–31.
[15] Grassi M, Zhang X. Finite element analyses of mode I interlaminar delamination in *z*-fibre reinforced composite laminates. Compos Sci Technol 2003;63:1815–32.
[16] Ratcliffe JG, Kruger RA. Finite element analysis for predicting mode I-dominated delamination growth in laminated structure with through-thickness reinforcement. In: Proceedings of American society for composites 21st annual technical conference. Dearborn, Michigan; 2006.
[17] Sankar BV, Hu S. Dynamic delamination propagation in composite beams. J Compos Mater 1991;25(11):1414–26.
[18] Sankar BV, Sonik V. Pointwise energy release rate in delaminated plates. AIAA J 1995;33:1312–8.
[19] Davila CG, Camanho PP, Turon A. Cohesive elements for shells. NASA-TP-2007-214869; 2007.